Hindawi
Mathematical Problems in Engineering
Volume 2019, Article ID 5747812, 11 pages
https://doi.org/10.1155/2019/5747812

Research Article

Research on the Improvement of Feedback Linearization Control in Suspension System Countering Inductance Variation

Liwei Zhang, Yue Zhang, Chao Zhang, and He Zhao

School of Electrical Engineering, Beijing Jiaotong University, Beijing 100044, China

Correspondence should be addressed to Liwei Zhang; lwzhang@bjtu.edu.cn

Received 8 February 2019; Revised 7 May 2019; Accepted 13 June 2019; Published 1 July 2019

Academic Editor: Alessandro Contento

The safety of the magnetic levitation (maglev) train is closely related to the control performance of the suspension module. However, during operation, the working conditions vary and are vulnerable to the external disturbances. In this work, a large-scale variation of the inductance of the magnetic levitation operation under different air gap conditions is considered, where the transfer function of the system changes nonlinearly. On the basis of the classical feedback linearization method, the algorithm of the first-order derivative for a single equilibrium point is improved, and then a multiequilibrium point feedback linearization method subject to the variation of the inductance is derived. The proposed linearization method can decouple the inductance from the air gap dynamics in any state of levitation, thus, reducing the model error. Using a general linear controller, the closed-loop control performance of the nonlinear hybrid excitation suspension system is run in MATLAB®. The simulation results show that the proposed method achieves good dynamic performance under various operating conditions and it improves the robust performance of the system.

1. Introduction

For urban low-speed magnetic levitation traffic, the hybrid excitation suspension electromagnet combines the permanent magnet excitation and the electric excitation and is connected in series in the magnetic circuit to generate a control voltage with a varying amplitude and direction through the winding to realize the magnetic circuit. The electric excitation control plays a role in adjusting the magnetic flux density, changing the magnetic attraction force, and adjusting the motion state of the system. Compared with the conventional electric excitation suspension magnet system, the most significant advantage of a hybrid excitation suspension system is energy savings, and the power required to the control system is small [1]. Studying hybrid excitation suspension system has important practical significance for improving the economic benefit and practical value of magnetic suspension technology.

In recent years, many scholars have conducted in-depth researches and discussions on the hybrid excitation magnetic levitation technology. Among the hybrid excitation control methods at the present, the Taylor series expansion about an equilibrium point is commonly used in the modeling approach [1–3]. However, at the positions that lie far away from the equilibrium point, especially during the course of events such as levitation and landing, the relative stability of the control system drops significantly. With the large-scale application of differential geometry in electrical control theory, nonlinear control methods have emerged. References [3–6] apply the state feedback linearization to magnetic levitation systems, and the control performance is improved compared with Taylor's linearization method. Among them, references [3, 4] use the current as the control input for being easily measured, but it does not represent the electromagnetic and dynamic changes inside the magnetic levitation system well. References [5, 6] use the air gap magnetic flux density as the internal control input that clearly describes the inherent law of the system. However, on this basis, it is necessary to install a magnetic density measuring device which is very rare in the field to form internal feedback of the system. Through the improvement of the above theoretical basis, references [7, 8] propose a feedback linearization control method based

on the rated operating point, which is a first-order derivative transformation process for the nonlinear system at the rated operating point. The simulation showed that the method is more robust to the uncertain systems.

Based on the feedback linearization method, references [9–13] robustly optimize the controller according to system characteristics and control requirements. In the design process, the control idea fully considers the uncertainties that appear inside and outside of the system, which include the system parameter perturbation, external noise, and high frequency interference. Combining the nominal and uncertain models with the robust controllers, the design optimization can be implemented for a given class of models. Compared with only considering the nominal model, this control method improves the conservativeness in the nominal design, but the system performance can be well-preserved under the parameter perturbation.

For systems that contain nonlinearities or potential bounded time-varying uncertainties, or systems that do not satisfy the global matching conditions, [9] propose an adaptive robust control method with state constraints which is suitable for the nonlinear maglev train suspension control. The method consists of a three-step state transition that converts the maglev train into an interconnected uncertainty system. And then, based on the proposed robust control of transformed system, the overall uncertainty of the adaptive law simulation system is constructed.

For the classes of fractional and integer-order systems with mismatched perturbations, a sliding mode control method based on a new fractional-order disturbance observer is proposed in [10]. This method can effectively handle the mismatched disturbance between quadcopters and the magnetic suspension systems, with better control performance, faster response, and reduced overshoot and jitter.

Reference [11] proposes a real-time adaptive control method suitable for large-scale mass change of magnetic levitation system. The method uses a fast internal current loop combined with adaptive control to manipulate the suspension control system, and even when the load weight varies widely, the system is still in a stable state.

In order to deal with the large-scale parameter perturbation changes, [12] performs inter-partition processing on the parameters. According to the experimental method, the weight functions of each segment are optimized separately to reduce the system conservativeness.

In [13], a Takagi-Sugeno (T-S) fuzzy controller based on the improved form of the piecewise Lyapunov function is used to relax the stability condition of the model, and the proposed method is combined with the Parallel Distributed Compensation (PDC) controller to stabilize the position of the magnetic ball in the magnetic suspension system under the disturbance. In addition, this technology ensures that the system is robust, the disturbance tolerance is maximized, the performance is improved, and the $\mathscr{H}_\infty$ performance metrics γ is reduced.

Based on [5, 6], this paper establishes a mathematical model of hybrid excitation single magnet. The differential geometry transformation in [6, 7] is used to obtain the classical Brunovsky's Canonical Form, and further first-order derivative operating is performed at the suspension equilibrium point to obtain a robust feedback linearization system. Based on the above linearization system, in the process of combining system air gap variation and the variation of the inductance value, the decoupling of system inductance value and the air gap change is proposed to improve the multiequilibrium point-based feedback linearization control method. The method can effectively cope with the model error caused by the variation of the system inductance and can improve the dynamic performance by real-time correction. Combining the linearization method proposed in this paper and the fundamental linear PID controller, the closed-loop control of the hybrid excitation suspension system is studied and verified through the MATLAB® simulation. In this simulation, the commands of levitation, square wave follower, and sudden load are given, and the common drift system parameter drift is simulated to investigate and compare the dynamic performance under different commands of each system. The simulation results demonstrate the effectiveness of the proposed linearization method.

2. Analytical Model

The research object of this paper is a hybrid excitation suspension module, which is mainly composed of long straight guide rail, electromagnet, and permanent magnet. The structure diagram is shown in Figure 1. In recent years, the low-speed maglev trains designed and manufactured in China use U-shaped magnet structures, which can be decoupled from the linear motor propulsion structure and more flexible in train control [1].

According to the working principle of the electromagnetic attraction, the air gap flux formula of the magnetic circuit of the hybrid excitation suspension module in Figure 1 is

$$\Phi(z,i) = \frac{F_m}{R_m} = \frac{\mu_0 A\left(Ni(t) + H_c h_{pm}\right)}{2z(t) + h_{pm}/\mu_r} \tag{1}$$

In Formula (1): $\boldsymbol{\Phi}$ is air gap flux; $\boldsymbol{F_m}$ is the total magnetomotive force; $\boldsymbol{R_m}$ is the total reluctance; μ_0 is the vacuum permeability; μ_r is the relative permeability; $\boldsymbol{A}$ is the electromagnetic attraction cross-sectional area; $\boldsymbol{z(t)}$ is the variable air gap; $\boldsymbol{i(t)}$ is the electric excitation current; $\boldsymbol{Hc}$ is the permanent magnet nominal coercivity; $\boldsymbol{h_{pm}}$ is the total thickness of the permanent magnet; $\boldsymbol{N}$ is the number of winding turns.

The formula for the electromagnetic attraction force without considering the magnetic flux leakage effect when the magnetic circuit passes through the air gap is obtained as

$$F(t) = \frac{B(t)^2 A}{\mu_0} = \mu_0 A\left[\frac{Ni(t) + H_c h_{pm}}{2z(t) + h_{pm}/\mu_r}\right]^2 \tag{2}$$

The system is controlled by the voltage input signal $\boldsymbol{u(t)}$. Assuming the circuit impedance is $\boldsymbol{R}$, the circuit formula is obtained as

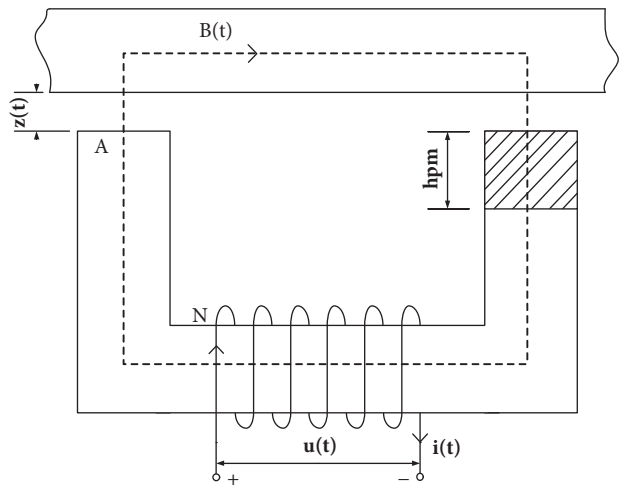

Figure 1: Schematic diagram of hybrid excitation.

$$u(t) = Ri(t) + \frac{d}{dt}\left[N\Phi(z,i)\right] = \frac{R}{N\mu_{pm}}\left[B(t)\cdot\left(2\mu_r z + h_{pm}\right) - H_c h_{pm}\mu_{pm}\right] + NA\dot{B} \quad (3)$$

In Formula (3), $\mu_{pm} = \mu_0.\mu_r$ is the permeability of the permanent magnet.

The dynamics of the suspension module is mainly affected by the electromagnetic attraction force $\boldsymbol{F(z,i)}$, the external interference $\boldsymbol{f_d}$, and the vehicle weight $\boldsymbol{Mg}$, where $\boldsymbol{M}$ is the vehicle mass and $\boldsymbol{g}$ is Earth's gravity:

$$M\frac{d^2 z(t)}{dt^2} = -F(z,i) + Mg + f_d \quad (4)$$

In this paper, the external disturbance force $\boldsymbol{f_d}$ is mainly composed of normal attraction $\boldsymbol{F_d}$. The permanent magnet synchronous linear motor above the suspension module will produce the interference effect under static or working conditions [14], so the suppression of this force is one of focal research points of this paper.

Figure 2 is the system open-loop control block diagram, obtained from Formulas (1) to (4).

3. Feedback Linearization

The state-space variables $\boldsymbol{x} = \begin{bmatrix} x_1 & x_2 & x_3 \end{bmatrix}^T = \begin{bmatrix} z(t) & v(t) & B(t) \end{bmatrix}^T$ are defined as the air gap, the vertical motion velocity, and the air gap flux density, respectively.

The suspension module described by Formulas (1)-(4) is a nonlinear system, and the system can be described as a mathematical model of a standard affine nonlinear system in the form of the following formulas:

$$\begin{aligned} \dot{x} &= f(x) + g(x)u \\ y &= h(x) \end{aligned} \quad (5)$$

$$f(x) = \begin{bmatrix} x_2 \\ g - \dfrac{A}{\mu_0 M}{x_3}^2 \\ \dfrac{R}{A\mu_{pm}N^2}\left[H_c h_{pm}\mu_{pm} - x_3\cdot\left(2\mu_r x_1 + h_{pm}\right)\right] \end{bmatrix} \quad (6)$$

$$g(x) = \begin{bmatrix} 0 & 0 & \dfrac{1}{NA} \end{bmatrix}^T$$

$$h(x) = x_1$$

$$u = u(t)$$

Since the relative order of this system is 3, which is equal to the system dimension, therefore, the system satisfies the controllability and the matching conditions and can be accurately linearized. By solving the Lie derivatives according to Formula (6), a new control variable $\boldsymbol{v}$ is obtained after the coordinate transformation. The control input voltage u_c of the original nonlinear system can be expressed as the following formula:

$$u_c = \alpha_c(x) + \beta_c(x)v = \frac{-L_f^3 h(x) + v}{L_g L_f^2 h(x)} \quad (7)$$

Note that $\boldsymbol{v}$ is a new control variable and is not the same as vertical motion velocity $\boldsymbol{v(t)}$. $\alpha_c(x)$ and $\beta_c(x)$ are defined in Formula (8), representing the constant term and the coefficient term, respectively, for the classical feedback linearization. In Formula (8), the other $\phi_c(x)$ is defined as the state variable vector group.

$$\begin{aligned} \alpha_c(x) &= -\frac{L_f^3 h(x)}{L_g L_f^2 h(x)} \\ &= -\frac{R}{\mu_{pm}N}\left[H_c h_{pm}\mu_{pm} - x_3\cdot\left(2\mu_r x_1 + h_{pm}\right)\right] \\ \beta_c(x) &= \frac{1}{L_g L_f^2 h(x)} = -\frac{\mu_0 NM}{2x_3} \\ \phi_c(x) &= \begin{bmatrix} x_1 & x_2 & g - \dfrac{A}{\mu_0 M}{x_3}^2 \end{bmatrix}^T \end{aligned} \quad (8)$$

The original nonlinear system (5) can be converted to the Brunovsky canonical form, and its affine transformed state variable $\boldsymbol{\phi_c}$ is expressed as

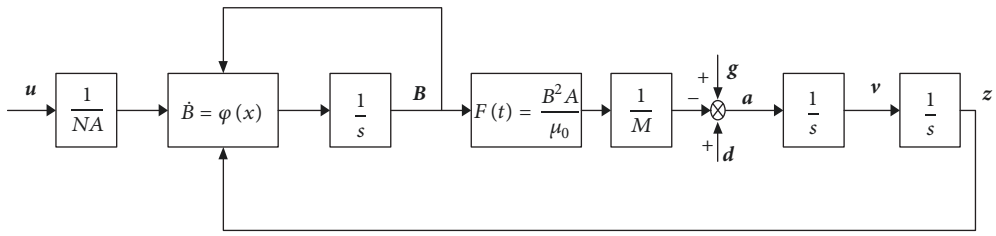

Figure 2: Open-loop control block diagram of the hybrid excitation suspension single iron system.

$$\dot{z} = \begin{bmatrix} 0 & 1 & 0 \\ 0 & 0 & 1 \\ 0 & 0 & 0 \end{bmatrix} z + \begin{bmatrix} 0 \\ 0 \\ 1 \end{bmatrix} v$$

$$y = \begin{bmatrix} 1 & 0 & 0 \end{bmatrix} z \tag{9}$$

$$z = \phi_c(x) = \begin{bmatrix} h(x) & L_f h(x) & L_f^2 h(x) \end{bmatrix}^T = \left[x_1 \quad x_2 \quad g - \frac{A}{\mu_0 M} {x_3}^2 \right]^T.$$

Note that z is the transformed coordinate and is not the same as the air gap $\boldsymbol{z(t)}$. The nominal transfer function g_{s1} of system (9) can be obtained as

$$g_{s1} = c(sI - A)^{-1} B = \frac{1}{s^3}. \tag{10}$$

4. Feedback Linearization Based on Rated Operating Point

During the implementation of the above control method, the nonlinear system is converted by the feedback linearization into a linear representation of the Brunovsky canonical form (9), which is a general result of any third-order SISO nonlinear system. In the subsequent model reference controller design, much of system information is hidden in the linearization transformation. Therefore, the feedback linearized model containing the physical information of the system must be obtained by means of the first-order derivative of the equilibrium operating point.

The Brunovsky canonical form (9) is expressed as

$$\dot{z} = Az + Bu. \tag{11}$$

where the state matrices $\boldsymbol{A_r}$ and $\boldsymbol{B_r}$ are the first-order derivatives of the system at the rated equilibrium point $x_0=[Z_0 \quad V_0 \quad B_0]^T$:

$$A_r \triangleq \left. \frac{\partial f}{\partial x} \right|_{x=x_0}, \qquad B_r \triangleq g(x_0). \tag{12}$$

Then the system control input $\boldsymbol{u}$ is

$$u(x, v) = \alpha(x) + \beta(x) v \tag{13}$$

where

$$\alpha(x) \triangleq \alpha_c(x) + \beta_c(x) Y T^{-1} \phi_c(x), \qquad \beta(x) \triangleq \beta_c(x) \left| H^{-1} \right|, \qquad \phi(x) \triangleq T^{-1} \phi_c(x) \tag{14}$$

In Formula (14), $\boldsymbol{\alpha, \beta, \phi}$ represent the constant term of the robust feedback linearization, the controller coefficient, term and the state variable vector group, respectively, and the variables are as follows:

$$G \triangleq L_g L_f^2 h(x_0), \qquad Y \triangleq -G \partial_x \alpha_c(x_0), \qquad T \triangleq \partial_x \phi_c(x_0), \qquad H \triangleq G^{-1} \tag{15}$$

where $\boldsymbol{G}$ is the second-order Lie derivative, $\boldsymbol{Y}$ is the partial derivative of $\boldsymbol{\alpha_c}$ at the equilibrium point and the product of-$\boldsymbol{G}$, $\boldsymbol{T}$ is the partial derivative of the state variable vector $\boldsymbol{\phi_c}$ at the equilibrium point, and $\boldsymbol{H}$ is the reciprocal of $\boldsymbol{G}$.

According to the original nonlinear system, the feedback linearization results based on the equilibrium point $x_0=[Z_0 \quad V_0 \quad B_0]^T$ are given by

$$A_r = \partial_x f(x_0) = \begin{bmatrix} 0 & 1 & 0 \\ 0 & 1 & \dfrac{-2AB_0}{\mu_0 M} \\ \dfrac{-2\mu_r B_0 R}{A\mu_{pm} N^2} & 0 & \dfrac{-\left(2\mu_r Z_0 + h_{pm}\right) R}{A\mu_{pm} N^2} \end{bmatrix}, \qquad B_r = \begin{bmatrix} 0 \\ 0 \\ \dfrac{1}{NA} \end{bmatrix} \tag{16}$$

According to Formula (13), the actual control input for the system, Formulas (17) and (18) can be derived:

$$\begin{aligned}\alpha(x) &= \alpha_c(x) + \beta_c(x) YT^{-1}\phi_c(x) \\ &= -\frac{R}{\mu_{pm}N}\left[H_c h_{pm}\mu_{pm} - x_3 \cdot \left(2\mu_r x_1 + h_{pm}\right)\right] \\ &\quad - \frac{2RB_0{}^2}{\mu_0 N}\frac{x_1}{x_3} \\ &\quad + \frac{\mu_0 RM}{2\mu_{pm}NA}\frac{1}{x_3}\left(g - \frac{A}{\mu_0 M}x_3{}^2\right)\left(2\mu_r Z_0 + h_{pm}\right)\end{aligned} \tag{17}$$

$$\beta(x) = \beta_c(x)\left|H^{-1}\right| = -\frac{B_0}{x_3}$$

$$\phi(x) = T^{-1}\phi_c(x) = \begin{bmatrix} x_1 \\ x_2 \\ \dfrac{-\mu_0 M}{2AB_0}\left(g - \dfrac{A}{\mu_0 M}x_3{}^2\right) \end{bmatrix} \tag{18}$$

According to the system state Formula (18), the transfer function g_{s2} is derived as (19)

$$\begin{aligned} g_{s2} &= C_r\left(SI - A_r\right)^{-1}B_r + d \\ &= \frac{-2B_0 A\mu_{pm}N}{\mu_{pm}\mu_0 MN^2 As^3 + RM\mu_0\left(2\mu_r Z_0 + h_{pm}\right)s^2 - 4AB_0{}^2 R\mu_r} \end{aligned} \tag{19}$$

Now, the transfer function g_{s2} containing the rich physical information of the system can be obtained, and the controller can be designed by the robust optimization method.

5. Multiequilibrium Point Feedback Linearization Method for Variation of Inductance Value of Suspension System

During the motion of the suspension system, the above feedback linearization system is based on the rated levitating air gap. Compared with the decoupled linearization system of the conventional motor, the inductance value changes nonlinearly in response to the levitating air gap, as shown in Formula (20) and Figure 3:

$$L = \frac{N^2 A\mu_0}{2z(t) + h_{pm}/\mu_r} \tag{20}$$

During the system levitation process, the air gap of the single magnet model is reduced from 0.025 m to the rated operating point of 0.01 m, and its inductance value is also changed from 0.17H to 0.03H. In other words, the suspension system is a strongly nonlinear system compared to the motor control system. The physical model of the system changes drastically throughout the start-up process. If the system only uses the transfer function based on the equilibrium point parameters, as Formula (19) shows, the deviation of the system characteristics will be generated at other operating points. Considering the above shortcomings, an improved multiequilibrium point feedback linearization method for the variation of the inductance value of the suspension system is obtained. This allows Formula (17) to be rewritten as the following formula:

$$\begin{aligned}\alpha_L(x) &= -\frac{R}{\mu_{pm}N}\left[H_c h_{pm}\mu_{pm} - x_3 \cdot \left(2\mu_r x_1 + h_{pm}\right)\right] \\ &\quad - \frac{2RB_0{}^2}{\mu_0 N}\frac{x_1}{x_3} \\ &\quad + \frac{\mu_0 RM}{2\mu_{pm}NA}\frac{1}{x_3}\left(g - \frac{A}{\mu_0 M}x_3{}^2\right)\left(2\mu_r z(t) + h_{pm}\right)\end{aligned} \tag{21}$$

$$\beta(x) = -\frac{B_0}{x_3}$$

The method replaces the rated operating point air gap $\boldsymbol{Z_0}$ in the $\boldsymbol{\alpha}$ term with a measurable air gap $\boldsymbol{z(t)}$. That is, at any time, ignoring the influence of nonlinear factors such as leakage inductance, the feedback linearization method can reproduce better dynamic characteristics of the original single-magnet nonlinear suspension system. The transfer function g_{s3} of the new feedback linearization method is shown in the following formula:

$$\begin{aligned} g_{s3} &= C_r\left(SI - A_r\right)^{-1}B_r + d \\ &= \frac{-2B_0 A\mu_{pm}N}{\mu_{pm}\mu_0 MN^2 As^3 + RM\mu_0\left(2\mu_r z(t) + h_{pm}\right)s^2 - 4AB_0{}^2 R\mu_r} \end{aligned} \tag{22}$$

The system's fixed value of $\boldsymbol{B_0}$ is only related to the load weight, independent of the system air gap, and the inductance is completely decoupled from the levitating state and position. Based on this method, a linear controller is designed, which can be added into the total controller of the nonlinear hybrid excitation suspension system. This particular closed-loop control block diagram is shown in Figure 4.

6. System Stability Analysis

In order to verify the stability of the feedback linearization system combined with the nonlinear magnetic levitation system, this paper carries out the following studies.

In Figure 4, the nonlinear magnetic levitation system processed by a robust feedback linearization method with inductance value decoupling can be expressed as a linear system, as shown in the following formula:

$$\dot{x} = A_r x + B_r u \tag{23}$$

The parameters of the maglev module are shown in Table 1.

According the Formula (16) and the parameters shown in Table 1, the specific expression of A_r, B_r can be obtained.

Table 1: The parameters of the maglev module.

Parameter		Value
Overall mass of the suspension	M (Kg)	650
Electric excitation winding number	N	200
Permanent magnet coercivity	H_C (Am)	8.8×10^5
Vacuum conductivity	μ_0 (H/m)	$4\pi\times10^{-7}$
Permanent magnet relative permeability	μ_r	1.05
Electric field winding resistance	R (Ω)	0.5
Permanent magnet radial length	h_{pm} (m)	0.02
Permanent magnet cross-sectional area	A (m^2)	0.0235
Gravity acceleration	g (m/s^2)	9.8

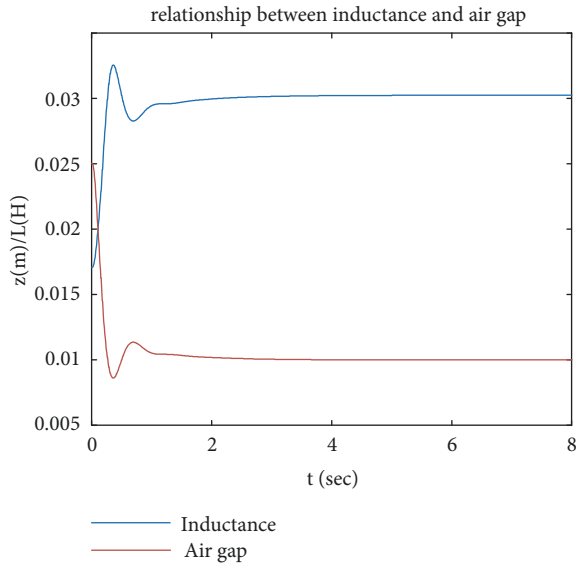

Figure 3: Relationship between single magnet suspension inductance and air gap.

$$A_r = \partial_x f(x_0) = \begin{bmatrix} 0 & 1 & 0 \\ 0 & 1 & -33.62 \\ -494.65 & 0 & -16.54 \end{bmatrix},$$
$$B_r = \begin{bmatrix} 0 \\ 0 \\ 4.7 \end{bmatrix} \tag{24}$$

The state feedback control is represented by k_1, k_2, and k_3, representing the feedback gains of the system state space variable system air gap x_1, velocity x_2, and acceleration x_3, respectively:

$$u = \begin{bmatrix} k_1 & k_2 & k_3 \end{bmatrix} \begin{bmatrix} x_1 \\ x_2 \\ x_3 \end{bmatrix} = k_1x_1 + k_2x_2 + k_3x_3 \tag{25}$$

Let the closed-loop system characteristic formula equal to 0.

$$\det(A_r + B_r u) = 0 \tag{26}$$

The following conditions can be gotten

$$\begin{aligned} k_1 &> -2324.855 \\ k_2 &> 0 \\ k_3 &< -77.738 \end{aligned} \tag{27}$$

That is, if the state feedback control parameter satisfies Formula (27), the closed loop system shown as Figure 4 is stable.

When the proposed feedback linearization method decouples the air gap inductance, the linearized system equation of the system will change monotonously with the air gap, and the parameter stabilization condition of the state feedback controller will change slightly. The control parameters used in this paper meet the stability requirements within the range of the model physical model.

The system is also analyzed by the Linear Analysis module of the MATLAB®/Simulink® software. The system transfer functions are shown in Table 2. The original nonlinear system with the equilibrium points of 0.01m, 0.0075m, and 0.0125m and the improved feedback linearization system Bode diagram are shown in Figures 5 and 6. The results show that the improved feedback linearization method can reproduce better frequency domain characteristics of the original nonlinear system.

7. Simulation

Based on the MATLAB®/Simulink® simulation platform, this paper simulates the working process of a magnetic hybrid excitation suspension module. The parameters of the system are shown in Table 1. The parameters of the PID controller are 10000, 10000, and 1500, respectively. The acceleration state feedback gain is -2600. To validate the algorithm, the same state feedback controller is used for the following four control systems:

ORI: the original nonlinear control system,

CFB: the classical feedback linearized control system,

RFB: the equilibrium point-based feedback linearized control system,

LRFB: the feedback linearized control system based on the improvement of the inductance value.

The control commands include the system response from the levitation to the rated operating point, the tracking of the

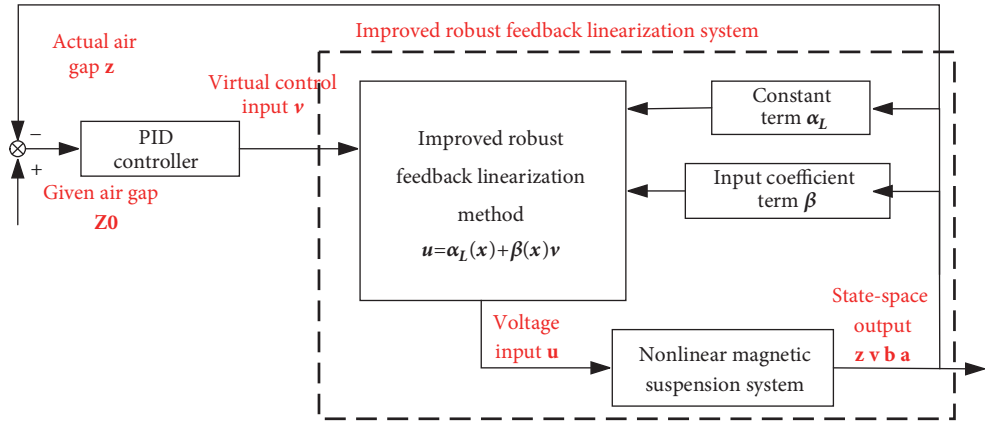

Figure 4: Improved robust feedback linearization method suspension system control block diagram.

Table 2: System transfer function.

Desired Air gap (m)	Original system	Improved feedback linearization system
0.01	$\frac{-7.145}{s^3 + 16.53s^2 - 1.659e4}$	$\frac{-7.15}{s^3 + 16.54s^2 - 1.661e4}$
0.0075	$\frac{-7.145}{s^3 + 14.41s^2 - 1.659e4}$	$\frac{-7.15}{s^3 + 14.42s^2 - 1.661e4}$
0.0125	$\frac{-7.145}{s^3 + 18.65s^2 - 1.659e4}$	$\frac{-7.15}{s^3 + 18.67s^2 - 1.661e4}$

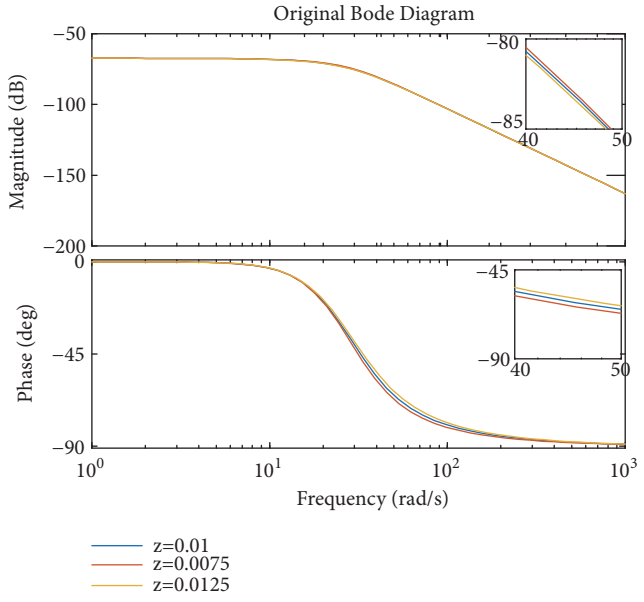

Figure 5: Original nonlinear system Bode diagram.

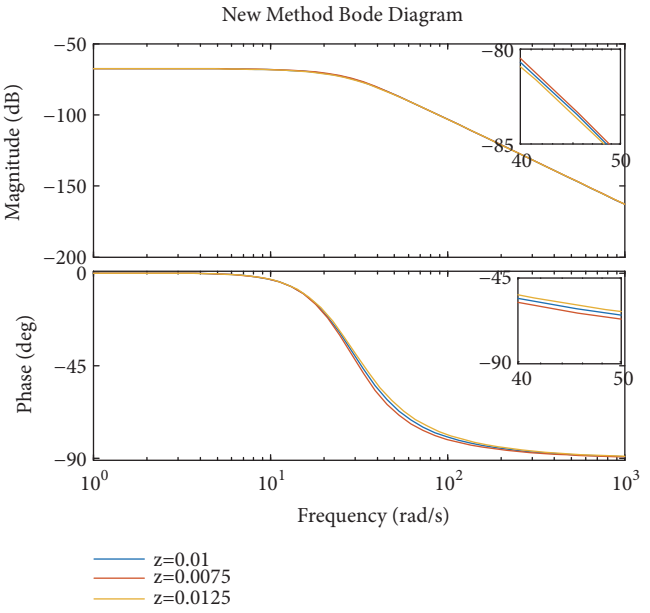

Figure 6: Improved feedback linearization system Bode diagram.

operating point, and the sudden load, as shown in Figures 7, 8, and 9.

In Figure 7, the system levitates from the initial position to the equilibrium point of 0.01 m. *RFB* and *LRFB* reach the steady-state with a small overshoot after 1 s, while *ORI* and *CFB* have a large overshoot (0.0075 meters) and reach the steady-state at 2.5 s after five damping oscillations.

In Figure 8, all four systems track the setpoints command from the equilibrium position (0.01 m) with a 1 Hz, a peak of 0.0125 meters, and a valley of 0.0075 m for motion. The

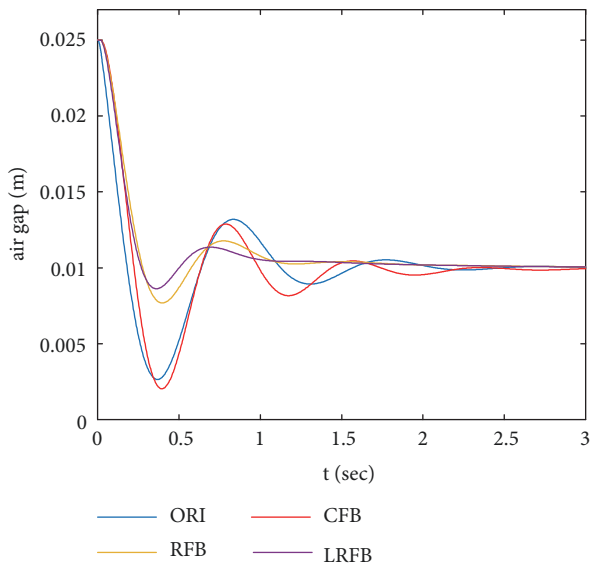

Figure 7: Levitation of the suspension system to the rated operating point.

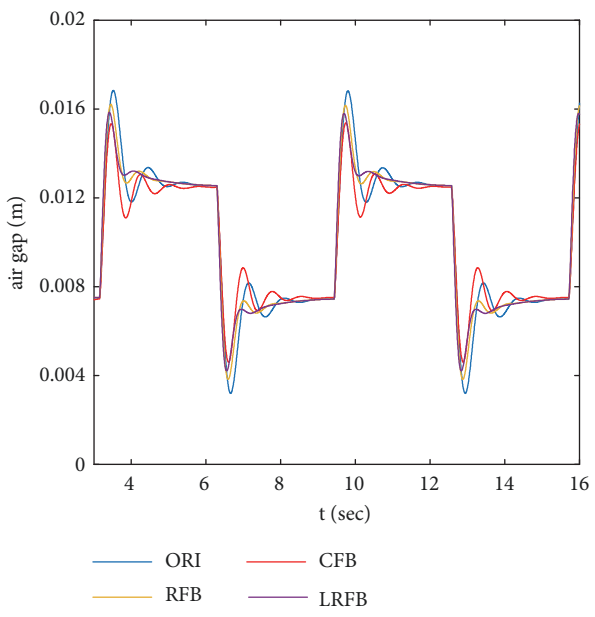

Figure 8: The suspension system tracks the rated working points.

responses of *ORI*, *RFB*, and *LRFB* follow the dynamic similarity of the system, leading to the amplitude of the levitation action decreasing in turn. Under the action of *CFB*, that is, the classical feedback linearization method, larger overshoots are generated during the even-number of overshoots, which is distinguished from the dynamic characteristics of the other three systems. The reason for the explanation *CFB* result is that *ORI*, *RFB*, and *LRFB* have similar system models, while *CFB* transforms the original system into $g_s = 1/s^3$, which weakens the dynamic control performance of the system to some extents.

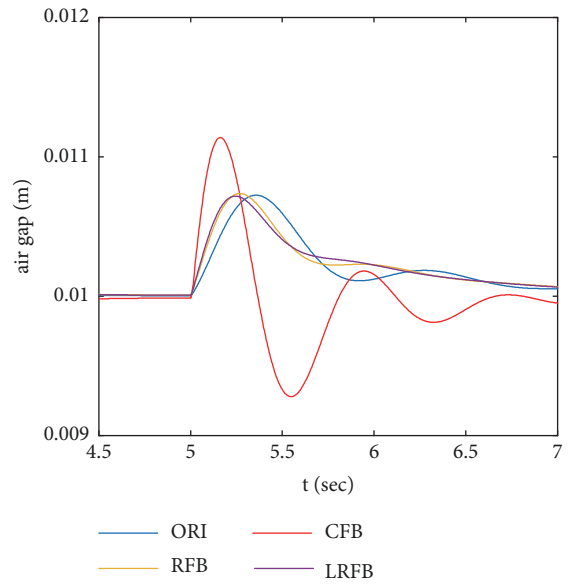

Figure 9: Response of a sudden load of the suspension system.

Figure 9 shows the response of the system to a sudden load of 0.2 kg under equilibrium. Similar to the above simulation, *ORI*, *RFB*, and *LRFB* have similar disturbance rejection characteristics. After 1s of transient time, *ORI*, *RFB*, and *LRFB* return to the equilibrium position, and the overshooting characteristic of *LRFB* is optimal (which means the lowest). After passing 2 s from 3.2 s, *CFB* achieves the maximum overshoot that is 1.5 times of the maximum overshoot of *LRFB*. However, CFB oscillates many times (only 2.5 oscillations are shown in Figure 9) before readjusting back to the equilibrium point.

The reason for the explanation of CFB's dynamical behavior is that when there is a sudden load, the model's system transfer function changes. Since the linearized models under the action of *RFB* and *LRFB* are closer to the nonlinear model after the load changes, then this explains the dynamical behaviors of *RFB* and *LRFB*. Similar to the *RFB*, the *LRFB* method can deal with the system disturbance that is caused by the mismatch of the model, better than the others. The mismatch happens when the magnetic levitation attraction is caused by the load variation, the external disturbance of gravity direction, or the leakage inductance. This verifies the system's robustness.

In order simulate the various conditions encountered in actual operation, a combination of parameter variations involving different types and states are applied. This helps to further verify the robust performance of the system. The simulation uses the sampling method for uncertain parameter combination that is specified by human operators. This method combines the uncertain parameter in the traversal way. Next, the simulation experiment is conducted in Simulink® repeatedly. Then, the results are summarized in the same observation coordinate system, and thereby, achieving the purpose of simulated random sampling. There are three parameters considered: the armature winding resistance R, which is greatly affected by the temperature; the coercive

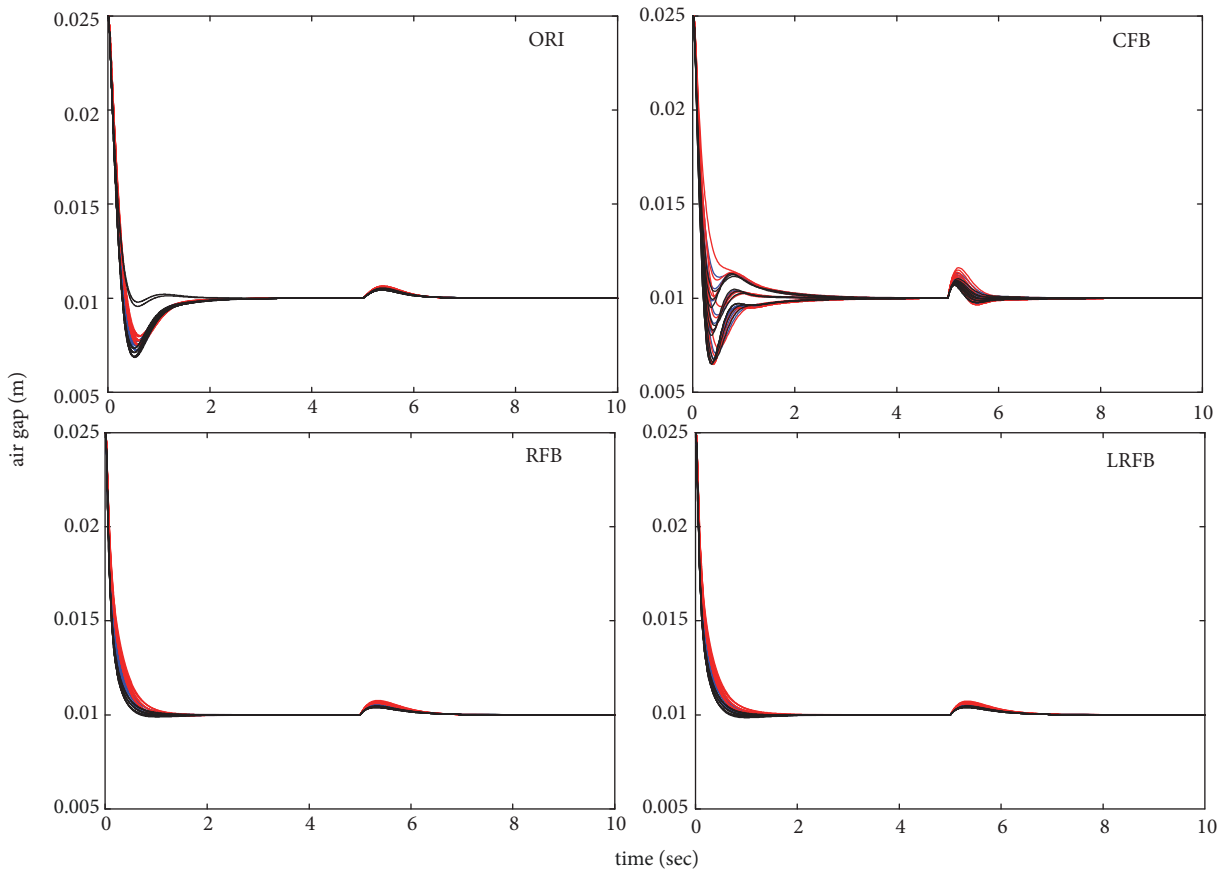

Figure 10: Dynamic response of system floating and step disturbance under multiple operating conditions.

force Hc of the permanent magnetic physical patch inside the hybrid excitation structure; and the levitated overall mass M.

Each parameter is taken one nominal quantity and two deviation quantities. Thus, there are a total of 27 parametric combinations of 3^3 variations.

The performances of the four different feedback linearization methods are analyzed after summarizing the effects of various possibilities on the dynamic responses of the magnetic levitation control system. In order to distinguish the variations of the suspension mass significantly up a certain degree, the specified 'nominal' mass $\mathbf{M_1}$ is labelled in Blue line, the total mass $\mathbf{M_2}$ (heavier than $\mathbf{M_1}$ by 20%) is labelled in Red line, and the total mass $\mathbf{M_3}$ (lighter than $\mathbf{M_1}$ by 20%) is labelled in Black line (see Figure 10). The specific variation parameters are shown in Table 3.

Figure 10 shows the dynamic response curves of the four linearization methods that are combined with the same linear controller for levitation and sudden load under multiple operating conditions. It can be seen that both *RFB* and *LRFB* maintain the consistency of the dynamic curves, and their overshoots are relatively small. However, *CFB* shows large inconsistencies of dynamical responses under different system parameter combinations, and their transient times are relatively longer. The maximum undershoot of *CFB* is about 25%. By directly controlling the suspension system with a linear controller, only two model curves of the specified mass achieve the nominal performances, and the others produce large undershoot.

Table 3: The parameters of maglev module.

Parameter		value
Overall mass of suspension	M_1 (Kg)	650
Overall mass of suspension	M_2 (Kg)	780
Overall mass of suspension	M_3 (Kg)	520
Electric field winding resistance	R_1 (Ω)	0.5
Electric field winding resistance	R_2 (Ω)	0.525
Electric field winding resistance	R_3 (Ω)	0.55
Permanent magnet coercivity	Hc_1 (Am)	8.8×10^5
Permanent magnet coercivity	Hc_2 (Am)	8.36×10^5
Permanent magnet coercivity	Hc_3 (Am)	7.92×10^5

Figure 11 shows the dynamic responses of the suspension system subjecting to the square wave command input under multiple operating conditions. In these cases, *CFB* also exhibits poor dynamic performance with the largest overshoot and the longest transient period. Comparatively, *ORI*, *RFB*, and *LRFB* perform better in tracking the square wave signal, but among them, dynamic responses of *LRFB* are the most definitive. The reason is that the upper and lower amplitudes of the square wave signal do not lie at the rated operating point, which enables the *LRFB* to change

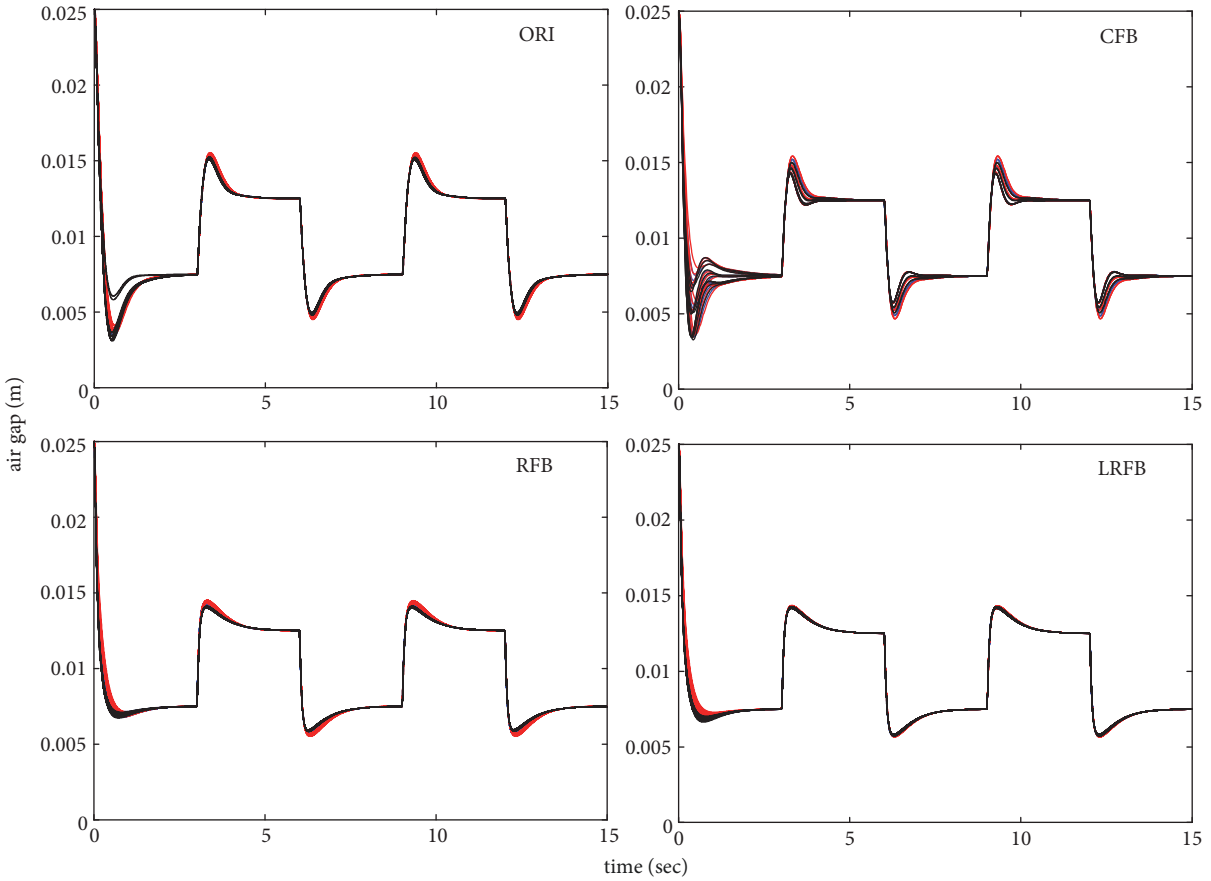

Figure 11: Dynamic response of system following square wave under multiple operating conditions.

the feedback coefficient according to the actual position of the system. This linearization method can reflect better system characteristics at the nonrated points. In particular, the inductance of the levitated magnet is decoupled to avoid modeling errors caused by different positions of the levitation.

8. Conclusion

This paper proposes a robust feedback linearization method based on the improved variations of inductance for the hybrid excitation magnetic levitation system. The proposed method is built on the basis of various control methods of feedback linearization in the reference. This method considers three things, namely, the levitation excitation of the hybrid excitation magnet, the different operating conditions, and the sensitivity of the system model to the inductance parameter error. This method can further improve the linearization of the system, making it closer to the dynamics of the original nonlinear system, therefore, enabling a more robust linear controller to be designed.

On the general basis of the linear controller and the same system modeling conditions, three different linearization methods are used to simulate the original nonlinear system. The results show that even in the presence of the internal system parameter drift and the external disturbances, the linearization method combined with the basic linear controller proposed in this paper can still maintain a nominal performance of the system. In other words, the proposed method has a certain degree of robust optimization effect on the linear controller of the front end. In this paper, the proposed method is beneficial to the enhancement of the system model details through the high precision feedback measurement of the state variables and the regulation of nominal system performance requirements. In addition, if the total mass of the suspension can be accurately measured, the dynamic performance of the system under heavy load or sudden load can be better guaranteed.

Data Availability

The Control Ideas of references ([1, 2, 6, 7, 9–14]) data used to support the findings of this study have been deposited in the [DOI] repository. The Control Ideas of references ([3–5, 8]) data used to support the findings of this study were supplied by [CNKI] under license and so cannot be made freely available. Requests for access to these data should be made to [CNKI, WWW.CNKI.COM.CN].

Conflicts of Interest

The authors declare that they have no conflicts of interest.

Acknowledgments

The project presented in this article is supported by National Key R&D Program of China (2016YFB1200601-B22).

References

[1] C. Hu, Z. Xiao, L. Yungang et al., "Analysis of control characteristics of electromagnetic permanent magnet hybrid suspension system," *Electric Drive for Locomotive*, vol. 2010, no. 2, pp. 18–21, 2010.

[2] M. Hypiusova and A. Kozakova, "Robust PID controller design for the magnetic levitation system: frequency domain approach," in *Proceedings of the 2017 21st International Conference on Process Control (PC)*, pp. 274–279, IEEE, Strbske Pleso, Slovakia, June 2017.

[3] C. Lei, *Research on hybrid suspension control method based on linear motor test platform [Doctoral thesis]*, Beijing Jiaotong University, 2008.

[4] L. Desheng, L. Jie, and W. Zhang, "Design of nonlinear levitation controller for EMS maglev train based on feedback linearization," *Journal of National University of Defense Technology*, vol. 27, no. 2, pp. 96–101, 2005.

[5] L. Hengkun, H. Aming, and C. Wensen, "Application of magnetic flux density feedback in magnetic levitation system," *Journal of National University of Defense Technology*, vol. 30, no. 6, pp. 129–133, 2008.

[6] W. Zhang, J. Li, K. Zhang, and P. Cui, "Design of Magnetic Flux Feedback Controller in Hybrid Suspension System," *Mathematical Problems in Engineering*, vol. 2013, Article ID 712764, 7 pages, 2013.

[7] A. L. D. Franco, H. Bourles, E. R. de Pieri, and H. Guillard, "Robust nonlinear control associating robust feedback linearization and H∞ control," *IEEE Transactions on Automatic Control*, vol. 51, no. 7, pp. 1200–1207, 2006.

[8] H. Guillard and H. Bourlés, "Robust feedback linearization," in *Proceedings of the 14th International Symposium on Mathematical Theory of Networks and Systems (MTNS'2000)*, pp. 1–6, Perpignan, France, 2000.

[9] X. Jinquan, D. Yutao, C. Ye-Hwa et al., "Adaptive robust constrained state control for non-linear maglev vehicle with guaranteed bounded airgap," *IET Control Theory & Applications*, vol. 12, no. 11, pp. 1573–1583, 2018.

[10] W. Jing, S. Changfeng, and C. Yang-Quan, "Fractional order sliding mode control via disturbance observer for a class of fractional order systems with mismatched disturbance," *Mechatronics*, vol. 53, pp. 8–19, 2018.

[11] Z. Zhang and X. Li, "Real-time adaptive control of a magnetic levitation system with a large range of load disturbance," *Sensors*, vol. 18, no. 5, article 1512, pp. 1–15, 2018.

[12] G. Cheng, Y. Yin, and C. Xinbo, "Robust control and optimization of rocker pusher electromagnetic active suspensions," *Automotive Engineering Magazine*, vol. 2018, no. 1, pp. 34–40, 2018.

[13] M. Khan and A. S. A. Mahmoud, "TS fuzzy controller of maglev system based on relaxed stabilization conditions," in *Innovations in Electronics and Communication Engineering*, vol. 7 of *Lecture Notes in Networks and Systems*, pp. 555–563, Springer, Singapore, 2018.

[14] T. Yongbin, L. Liyi, L. Jiayu et al., "Thrust analysis of non-core permanent magnet linear synchronous motor with fractional slot centralized winding," *Journal of Electric Machines and Control*, vol. 17, no. 8, pp. 1–8, 2013.